



Nutrient fluxes from upwelling and enhanced turbulence at the top of the pycnocline in Mono Lake, California

Sally MacIntyre & Robert Jellison

Marine Science Institute, University of California, Santa Barbara, CA 93106-6150, U.S.A.

Key words: Turbulence, phytoplankton, nutrients, stratification, nutrient limitation

Abstract

Time series measurements of temperature at 15 depths and profiles of temperature-gradient microstructure were obtained during a period with strong wind forcing and subsequent calm in Mono Lake, California. The wind forcing increased the amplitude of basin-scale internal waves and energy at all wave frequencies relative to the calm period. Rates of dissipation of turbulent kinetic energy, ϵ , were high ($\epsilon > 10^{-6} \text{ m}^2 \text{ s}^{-3}$) at the top of the pycnocline at both an inshore and an offshore site on a day when winds reached 10 m s^{-1} and on the following two days at an inshore site ($\epsilon > 10^{-7} \text{ m}^2 \text{ s}^{-3}$). The enhanced turbulence occurred at the depth of a subsurface temperature maximum (z_{TM}) and coincidentally with elevated concentrations of NH_4 , reduced concentrations of chlorophyll *a* and particulate carbon, and increased abundance of the macrozooplankter *Artemia monica*. The NH_4 at z_{TM} was more dispersed and of lower concentration inshore than offshore and indicated greater turbulent transport inshore. Over the course of 4 days, chlorophyll *a* concentrations increased in the upper mixed layer, and C:N and C:Chl ratios decreased. Offshore, the change in C:N ratio indicated a relaxation of moderate nutrient deficiency. We hypothesize that excretion by *A. monica* and turbulent transport of the NH_4 from the subsurface temperature maximum led to improved physiological status of phytoplankton in the upper mixed layer.

Introduction

A lake's overall productivity depends, in part, on the supply of both nutrients and light. Supply and availability of these resources in a lake is governed by several factors, including geological setting, lake morphometry, biological interactions, and, in large part, the hydrodynamical processes that are driven by climatic forcing. In the last 15 years our understanding of these hydrodynamical processes, particularly those that occur during stratified periods, has increased substantially due to an increase in field and laboratory experiments plus the advent of new instrumentation (Imberger, 1985; Imberger & Patterson, 1990; Imberger & Ivey, 1991; Saggio & Imberger, 1998).

Key hydrodynamical processes that affect ecosystem functioning include those induced by wind and those induced by heating and cooling at the lake's surface (Fig. 1). Of central importance for primary productivity and biogeochemical processes are the turbulent eddies that redistribute nutrients, gases and organisms. Those in the upper mixed layer deter-

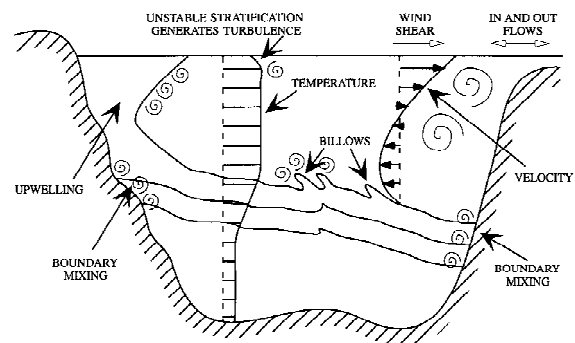


Figure 1. Key hydrodynamic processes in stratified lakes, redrawn from Svensson (1978). Turbulent eddies from wind mixing and surface cooling and currents induced by wind occur at all times of year. Other processes only occur when water bodies are stratified. In particular, internal waves are generated whose interaction with topography creates instability and mixing. Horizontal flows are induced by intrusions from boundary mixing, stream inflows, and by differences between rates of heating and cooling and wind mixing between the pelagic and littoral zone.

mine the light exposure of phytoplankton (Patterson, 1991; MacIntyre, 1993, 1998). They may entrain

nutrient-rich waters from the metalimnion leading to higher rates of primary productivity in the upper mixed layer (Jellison & Melack, 1993a). Turbulence in the metalimnion is caused by shear due to internal wave motions and by breaking internal waves (Thorpe, 1978, 1998). If nutrient concentrations are elevated in the metalimnion, mixing will cause increased nutrient supply to the upper mixed layer.

Recently, it has been recognized that turbulence near basin boundaries and topographic features can be an order of magnitude or more higher than turbulence offshore (Goudsmit et al., 1997; Polzin et al., 1997; MacIntyre et al., 1999). This turbulence may be induced by current or wave induced shear stresses at the sediment–water interface, by breaking internal waves, or by wave–wave interactions caused by wave reflection or interaction with topography (Thorpe, 1984, 1987, 1989, 1998; DeSilva et al., 1997; Maxworthy et al., 1998). The turbulence may transport nutrients or gases vertically from the nutricline (MacIntyre et al., 1999), cause entrainment of sediments (Gloor et al., 1994), and may entrain nutrient-rich pore waters. The resulting well-mixed water may then flow offshore as intrusions along isopycnals (surfaces of equal density) or may be transported by gyres (Melack & Gastil, 2001).

While vertical transport is critical for many biological processes, it only occurs if the magnitude of the rate of dissipation of turbulent kinetic energy exceeds damping forces due to viscosity ν and buoyancy as indicated by the buoyancy frequency, $N = (g/\rho \partial\rho/\partial z)^{1/2}$ where ρ is density g is gravity, and z is depth. In laboratory and field studies, Ivey & Imberger (1991) and Itsweire et al. (1993) determined that buoyancy flux, that is vertical mixing of stratified waters, would occur when $\epsilon > 15\nu N^2$. Recent field results have shown a somewhat lower threshold: $\epsilon > 6\nu N^2$ (Saggio & Imberger, 2001). Other recent field results have shown that overturning scales, that is the size of turbulent eddies, are small in the pycnocline in offshore waters despite rates of dissipation of turbulent kinetic energy at which turbulent transport is expected (Etemad-Shahidi & Imberger, 2001). The coefficient of eddy diffusivity K_z , a term used to indicate turbulent transport in a stratified flow, is proportional to turbulent velocity u and length l scales ($K_z \sim ul$, Tennekes & Lumley, 1972). When length scales are small, K_z will be small and transport limited. The vertical flux of solutes and gasses will be limited if ϵ does not exceed a threshold value or if overturning scales are on scales less than centimeters.

We have conducted two studies in Mono Lake, California, to determine fluxes due to mixing at the boundaries. MacIntyre et al. (1999) showed that turbulence was up to four orders of magnitude higher inshore than offshore. Due to the large vertical gradient in NH_4 at the depths of mixing, the calculated flux of NH_4 was sufficient to support daily rates of primary productivity throughout the lake at the depth of the chlorophyll maximum. However, whether fluxes actually occurred was not evaluated in this study. We found that the frequency of turbulent events in which ϵ exceeded a threshold of $15\nu N^2$ was greater inshore than offshore, a finding that would suggest greater transport would occur inshore. In our second study, we used a conservative tracer (SF_6) as well as microstructure profiling to determine whether turbulent transport was greater at the boundary. While we could not determine where the dispersion of SF_6 was greater, we did find that approximately an order of magnitude more tracer was transported through the pycnocline during a 2-day storm event than during six calm days (MacIntyre et al., unpublished data). Our microstructure results linked the incidence of turbulence with enhanced wind forcing as well as bottom slope. Shortly after the passage of a front with winds in excess of 10 m s^{-1} , 90% of the metalimnion was turbulent near an island where bottom slopes ranged from 0.07 to 0.1 m m^{-1} , 30% of the water column was turbulent inshore where bottom slopes were 0.02 m m^{-1} , and less than 6% of the water column was turbulent offshore where bottom slopes were 0.002 m m^{-1} . Six days later, when diurnal winds with speeds of 5 m s^{-1} had become established, only 30% of the metalimnion was turbulent near the island, less than 12% inshore, and 2% offshore.

While these previous studies of turbulence in Mono Lake documented the increased turbulence in the metalimnion over sloping topography and showed increased solute flux with high winds, they have not demonstrated where fluxes are highest. Nor have they established a relation between turbulence and the energy in the internal wave field or the magnitude of solute fluxes.

In the following, we further analyze the physical, chemical and biological data collected in October 1995 (MacIntyre, 1998; MacIntyre et al., 1999) with an emphasis on internal wave dynamics, the enhanced turbulence at the top of the pycnocline, and inshore and offshore differences in nutrient fluxes from the pycnocline into the upper mixed layer. We illustrate the internal wave structure for 2 days with high winds and 2 days with calm, compare the energy at differ-

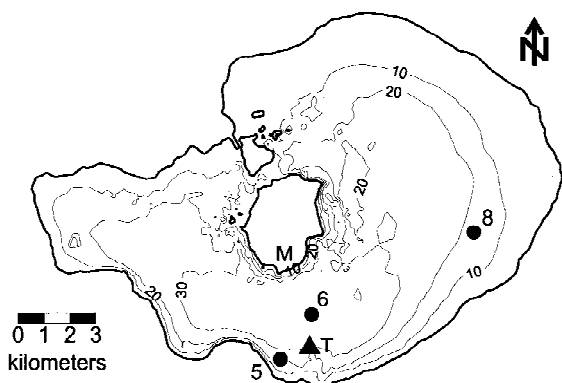


Figure 2. Bathymetric map of Mono Lake showing the location of the meteorological station M on Paoha Island, the thermistor chain T (\blacktriangle), and locations of sampling (\bullet) inshore (stations 5 and 8) and offshore (station 6). Contour intervals are in meters.

ent wave frequencies for these 4 days, and relate the incidence of turbulence to the wave forcing. In addition, we present time series data on distributions of NH_4 , chlorophyll *a*, and carbon to nitrogen (C:N) and carbon to chlorophyll (C:Chl) ratios at inshore and offshore sites. Based on the distributions of NH_4 and chlorophyll *a*, we infer whether vertical mixing occurred at inshore and offshore sites, and from changes in C:N and C:Chl ratios we determine whether the physiological status of the phytoplankton improved due to the wind forcing. Using coefficients of eddy diffusivity calculated from temperature-gradient microstructure profiles, we calculate fluxes of ammonia from the top of the pycnocline and assess their likely contribution to growth. We use the combined data to infer whether turbulent transport actually occurred in Mono Lake, and if so, where.

Study site

Mono Lake (38° N, 119° W) is a terminal saline lake located in the Great Basin east of the Sierra Nevada (Fig. 2). In October 1995, when the surface was 1944 m, its surface area was 171 km^2 and its maximum depth was 46 m. During the last two decades, Mono Lake has alternated between monomixis and meromixis as the lake's level rose and fell due to variability in snowmelt runoff and diversions of water in the basin. At higher lake levels when the monimolimnion has been freshened, the density stratification across the pycnocline is strengthened and the lake is more resistant to turbulent mixing (Romero et al., 1998; MacIntyre & Romero, 2000). Consequently, primary

productivity is depressed due to reduced nutrient loading from the monimolimnion (Jellison & Melack, 1993a). A rise in lake level occurred in 1995 and initiated an extended period of meromixis.

Descriptions of the lake's thermal and chemical structure, primary and secondary productivity, and vertical mixing processes are provided by Jellison & Melack (1988, 1993 a,b, 2001), Jellison et al. (1993), Melack & Jellison (1998) and Romero & Melack (1996). Mono Lake has few phytoplankton species and one dominant zooplankton species, the brine shrimp *Artemia monica* Verill. As this paper extends MacIntyre et al. (1999), many relevant details are presented there and in MacIntyre (1998), including high resolution temperature profiles and profiles of rates of dissipation of turbulent kinetic energy.

Gyres with elevated abundance of chlorophyll are a common feature in Mono Lake in late summer and early fall. Imagery from airborne imaging spectrometry indicated a gyre was present in the northeastern portion of the lake on 10 October 1995, the day prior to our sampling (Melack, in press). The technique is described in Melack & Gastil (2001).

Methods and calculations

Physical measurements

Meteorological and radiation measurements are described in MacIntyre et al. (1999). The station was located at the southern shore of Paoha Island; each sensor was sampled every second, and data were stored as ten-minute averages. Attenuation of photosynthetically available radiation (PAR) within the water column was measured with a submersible Licor sensor (model LI-192S sensor, model LI-185 meter) at 0.5-m intervals.

Temperature-gradient microstructure and conductivity, temperature and depth (CTD) measurements are described in detail in MacIntyre et al. (1999). Temperature, temperature gradients, conductivity and pressure were measured at a frequency of 100 Hz using temperature-gradient microstructure profilers (Self-Contained Autonomous Microstructure Profiler or SCAMP, Precision Measurement Engineering). A CTD (Sea-Bird Electronics, Seacat Profiler, SBE-19) also was used for profiles of temperature and conductivity. Time-series measurements of temperatures at 15 depths were obtained with self-contained temperature loggers (WaDaRs, TSKA Inc.) deployed on a subsurface mooring near Station 5 (Fig. 2). Each WaDaR

has an accuracy of 0.001°C , a resolution of 1.4 mdeg, and a time constant of ~ 3 min.

Chemical analysis

Ammonium ($\text{NH}_4^+ + \text{NH}_3$) concentrations were measured by the indophenol-blue method (Strickland & Parsons, 1972). Chlorophyll *a* was determined by spectrophotometric analysis with correction for phaeopigments (Golterman, 1969). Details for both procedures are given in Jellison et al. (1993). Particulate organic carbon, phosphorus and nitrogen were measured after samples were filtered through precombusted Gelman A/E filters. Methods are provided in Jellison & Melack (2001).

Calculations

Density was calculated from temperature and conductivity corrected to 25°C using an equation of state developed for Mono Lake (Jellison et al., 1999). Density profiles from the SCAMP were calculated using data from a fast response (Thermometrics FP07) thermistor and the larger conductivity sensor. The fast response thermistor was filtered to match the time constant of the larger conductivity sensor (180 msec) and offset by 0.4 s so values from both sensors were from the same location. For the CTD profiles, density was computed after averaging the conductivity profiles over 1-m intervals centered on every meter; corresponding temperatures at each meter were obtained from interpolated temperature profiles.

Rates of dissipation of turbulent kinetic energy (ϵ) were computed by a least-squares fit of the power spectral densities of the temperature-gradient signal to the Batchelor spectrum (Dillon & Caldwell, 1980; Imberger & Ivey, 1991). Power spectral densities were calculated in segments as described in MacIntyre et al. (1999). The procedure is an adaptation of that described in Imberger & Ivey (1991) and is used to determine where the turbulence is statistically stationary (Imberger & Ivey, 1991). Vertical eddy diffusivity, K_z , was calculated using Osborn's (1980) model, $K_z = \Gamma \epsilon N^{-2}$, where Γ is the mixing efficiency and N is the buoyancy frequency. We let $\Gamma = 0.25$, the upper limit in Ivey & Imberger's (1991) analysis and similar to the mean mixing efficiency of 0.265 found by Oakey (1985). We calculated the flux of ammonium as $F = K_z \partial[\text{NH}_4]/\partial z$.

Arithmetic averages of ϵ and K_z were determined for 1 m intervals by determining the percentage of the interval occupied by a segment, multiplying that

percentage by ϵ for that segment, summing the contributions from each segment, and assuming that ϵ equaled $10^{-10} \text{ m}^2 \text{ s}^{-3}$ and K_z equaled $10^{-9} \text{ m}^2 \text{ s}^{-3}$ where the water column was not turbulent. The first of these two values reflects instrument threshold for turbulence and the second the rate of molecular diffusion of salts. Depth-averaged values of ϵ and K_z were computed for each site on each day. Estimates of K_z based on the assumption of a log normal distribution of turbulent events (MacIntyre et al., 1999) were equivalent to arithmetic averages at the depths where we calculated ammonia fluxes.

Isotherm depths were determined using linear interpolation between the depths of the thermistors. Power spectral analyses of the isotherm displacements were computed using a Hanning window and linear detrending. Eighty percent confidence intervals were computed and windows overlapped 75%. To generate smaller confidence intervals at higher frequencies, we decreased the size of our windows as frequencies increased. Power spectral densities were multiplied by the mean buoyancy frequency at the depth of the isotherm so the results would be equal to the potential energy density of the internal wave field. The magnitude of isotherm displacements, δ , at low, moderate and high frequencies were determined using band-pass filtering using an inverse fast Fourier transform. Potential energy per unit mass was calculated for each frequency band as $N^2 \delta^2$ as in Moum et al. (1992).

Results

Wind forcing and thermal, conductivity, and density structure

High winds occurred at the beginning of our study period (Fig. 3A), with magnitude exceeding 10 m s^{-1} on 11 October for about 7 h and exceeding 8 m s^{-1} for about 7 h on 12 October. These winds generated upwelling and downwelling of the pycnocline (Fig. 3B) with maximum displacements of 1.5 m where displacements are the distance from crest to trough. The largest amplitude internal waves occurred on 11 and 12 October.

A subsurface temperature maximum is conspicuous in the time series record. It was located initially at 9 m depth and subsequently at 10 m depth or slightly lower (Fig. 3B). Over the 4-day period, the subsurface temperature maximum was initially about 2 m thick; by the end of the study, it had thinned to 0.5

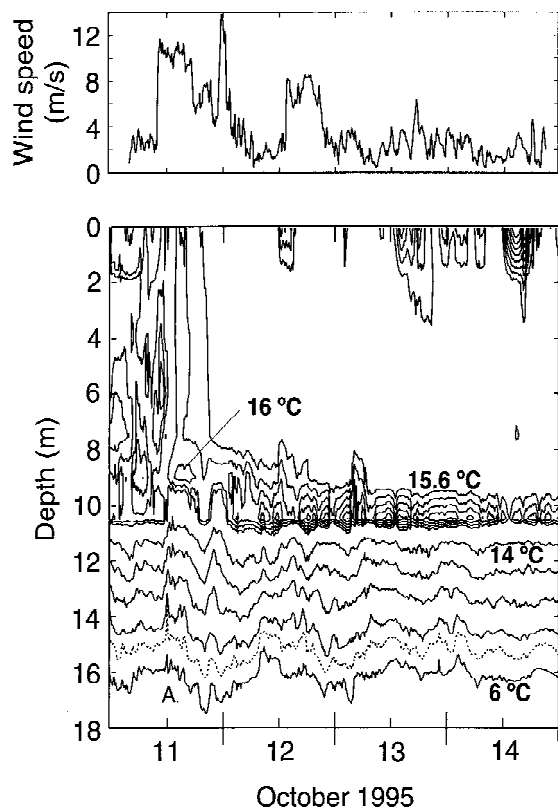


Figure 3. (A). Wind speed as 10 min averages 11–14 October 1995. (B). Isotherms for the same period showing the initial patchiness of temperature in the upper mixed layer above 8 m depth and its reduction due to cooling from winds, the subsurface temperature maximum near 10 m depth, the internal wave activity in the pycnocline including the initial large upwelling whose initiation is marked by the letter A, and the diurnal heating in the upper part of the upper mixed layer on 12–14 October. Temperature contours are 2 °C in the pycnocline, and 0.02 °C in the temperature maximum. 7 °C isotherm is dotted.

m. Pockets of warmer water occurred intermittently in the subsurface temperature maximum, and within the upper mixed layer on 11 October. We call the depth of the subsurface temperature maximum z_{TM} .

The chemocline, which began at 8 m depth, stabilized the water column where the temperature was inversely stratified (Fig. 4A). The profile of density was similar to conductivity, with the pycnocline extending from 8 to 17 m. We define the upper mixed layer as that portion of the water column above 8 m. It was weakly stratified, and as will be seen below, was not always turbulent.

Internal waves

Spectral analysis of temperature records for the 2 week study in 1999 indicated that the most energetic, lower frequency waves had periods of about 1 day and were likely a second vertical mode internal wave that propagated around the boundary of the lake (MacIntyre et al., 1999). Energies were also elevated at periods of 8 h, the period of a first vertical mode wave. For a first vertical mode wave, the top and bottom of the pycnocline remain parallel as the pycnocline up and downwells. For a second vertical wave mode, the movements of the top and bottom of the pycnocline are 180° out of phase.

Turbulence at the margins of lakes and oceans is expected to occur due to breaking of waves at critical frequencies, $f_c = N\beta$ where N is the buoyancy frequency and β is the bottom slope (DeSilva et al., 1997). Finding an increase of energy at those frequencies at the same time as rates of dissipation of turbulent kinetic energy are increased would provide evidence that internal wave breaking at the bottom boundary is contributing to the turbulence. At our inshore site, critical frequencies ranged from 2 to 168 cpd. Given the high values of N at the top of the pycnocline, and a typical bottom slope of 0.02, critical frequencies will center around 34 cpd. At 15 m, where turbulence was enhanced at the base of the pycnocline, critical frequencies will center around 19 cpd.

To determine if the energy in the internal wave field changed in response to wind forcing and if energy became elevated at critical frequencies, power spectral analysis of isotherm displacements were determined for three 36 h periods: the initial period of wind forcing (11 October to noon 12 October), after the second wind event (noon 12 October to 0000 h 14 October), and after winds decreased (14 October to noon 15 October) (Fig. 5). The length of these records is too short to show the energy in the lowest frequency basin-scale waves but is long enough to show energy throughout the range of critical frequencies as well as higher frequencies. Because of the temperature maximum at the top of the pycnocline, isotherm displacements cannot be calculated there. Instead, we present analyses for the 14 °C isotherm, the uppermost one that can be calculated. For this isotherm, at ~11 m depth, energies are comparable at all frequencies for the first two periods but are an order of magnitude less in the third. Power spectral analysis of the 7° isotherm, ~15 m depth, also showed energy enhancement at critical frequencies and higher for the first two periods and a

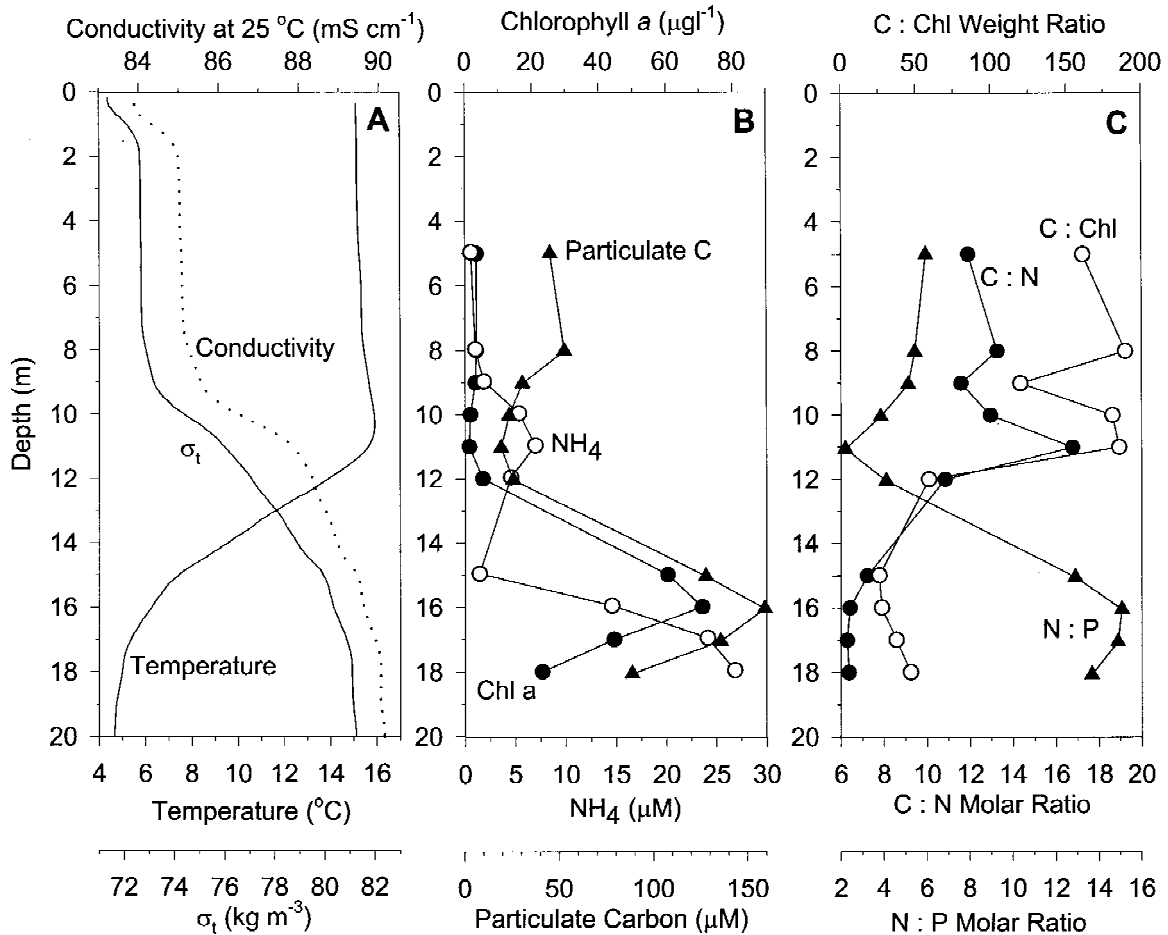


Figure 4. (A). Profiles of temperature, conductivity and density at Station 6 at 0707 h 12 October 1995. The subsurface temperature maximum between 8 and 11 m depth is stabilized by the increased conductivity. Data were obtained by a SeaBird CTD. (B). Profiles of NH₄, chlorophyll *a*, and particulate carbon (PC) at 0745 h 12 October show the increased NH₄ concentrations and reduced chl *a* and particulate carbon at the depths of the subsurface temperature maximum. (C). Profiles of C:N, C:Chl, and N:P at 0745 h illustrating the subsurface maximum of the C:N and C:Chl and minimum of N:P at z_{TM} .

decay in energy by an order of magnitude by the third period (not shown).

Isotherm displacements were band pass filtered in four frequency ranges (Fig. 6A,C,E). The first, 0.07–2.4 cpd, indicates the thermocline deflections due to basin scale waves. The second, 2.4–19.2 cpd, illustrates the deflections due to the first vertical first horizontal wave and higher harmonics of this wave and other basin scale waves. The third, 19.2–192 cpd, shows deflections at higher frequencies within the range critical for wave breaking at the boundary. Frequencies higher than critical (192–600 cpd) comprise the fourth frequency range. The response of the basin scale waves to wind forcing differed between the top and base of the pycnocline. At the top, the major up

and downwelling persisted for a day and a half with the overall deflection 1.2 m (Fig. 6A). In contrast, for the 7 °C isotherm at about 15 m, the amplitude was similar but the wave went through a cycle and a half before decaying. At the base of the pycnocline, the amplitude was larger and increased with time. Waves with frequencies of 19.2–192 cpd initially had 1 m deflections, but they decreased after 13 October. Waves in this frequency range are critical for breaking if slopes are ≥ 0.02 . Packets of waves in the frequency band from 19.2 to 192 cpd were always present, but their amplitudes increased intermittently. The amplitude of waves in the highest frequency band tended to increase at the same time as those with frequencies of 19.2–192 cpd.

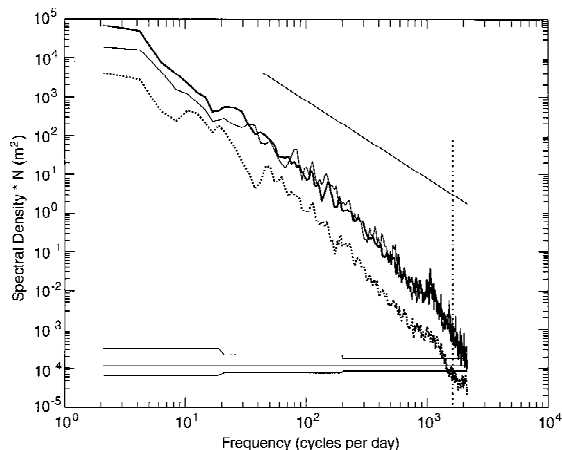


Figure 5. (A). Power spectrum of 14 °C isotherm multiplied by N shows that the internal wave field contained more energy during the first three days of the study than during the subsequent day and a half. Power spectra were computed for 0000h 11 October to 1200 h 12 October (thick solid line), 1200 h 12 October to 0000 h 14 October (thin solid line), 0000 h 13 October to 1200 h 15 October (dashed line). Line in upper right has slope of -2 , as is typical for oceanic waters and large lakes. 80% confidence intervals are indicated by stepped lines for which windows (2048, 1024 and 512) were decreased as frequency increased to improve confidence. Dotted vertical line indicates buoyancy frequency.

The decay in potential energy density from 11 and 14 October occurred at all frequencies on the 14 and 7 °C isotherms, whereas the energy persisted longer in basin scale modes on the 5 °C isotherm (Fig. 6B,D,F). This isotherm was at the base of the pycnocline and also intercepted the bottom. The energy in the highest frequency waves decayed more rapidly there.

Turbulence

Rates of dissipation of turbulent kinetic energy in the upper part of the water column were higher when winds were stronger, whereas those below z_{TM} had a delayed response to wind forcing (Fig. 7). Sampling on 11 October occurred during the initial period of wind forcing. Nearly the entire upper 10 m was turbulent at both locations, with $10^{-8} < \epsilon < 10^{-5} \text{ m}^2 \text{ s}^{-3}$. Inshore, turbulence was enhanced between 6 and 9 m, where the nutrient time series (see below) indicates upwelling occurred. Below z_{TM} inshore, the turbulence was intermittent, only infrequently as high as $10^{-8} \text{ m}^2 \text{ s}^{-3}$, and was slightly enhanced at the bottom. Offshore, the turbulence was even more intermittent and the highest values occurred in the upper part of the pycnocline.

On 12 October, sampling offshore began just before the winds increased, and the low values of ϵ near the surface in the first few profiles reflect the low winds. The water column had two distinct regions with higher dissipation rates: the upper portion that was directly energized by wind and mid-water column in a 4 m swath above and below z_{TM} . Within the pycnocline, $10^{-9} < \epsilon < 10^{-7} \text{ m}^2 \text{ s}^{-3}$. Inshore, ϵ was elevated in the upper 3 m. The pycnocline was highly energized above and below z_{TM} . Values of ϵ in the bottom 3 m equaled the high values at z_{TM} .

Wind forcing was moderate on 13 October, but the same patterns occurred in the distribution of ϵ . Values were highest in the upper part of the water column although the depth of enhanced turbulence near the surface was shallower. The upper 65 cm were not included as profiles were downcasts. Elevated turbulence at the temperature maximum occurred inshore and offshore, but ϵ was lower than on the previous two days. Enhanced dissipation occurred near the bottom inshore. Turbulence also occurred deep within the monimolimnion offshore.

Light and oxygen

Daily maxima of photosynthetically available radiation (PAR) at the surface was $1500 \mu\text{E m}^{-2} \text{ s}^{-1}$ and the euphotic zone, defined as the depth at which irradiance is 1% of surface values, was 14 m. The oxycline was between 5 and 12 m, 10 and 14 m, and 10 and 15 m on 11, 12 and 13 October, respectively.

Nutrients and chlorophyll distributions

Typical profiles of NH_4 , chlorophyll a and particulate C are illustrated for the offshore station in Figure 4B; ratios of particulate carbon to particulate nitrogen (C:N), particulate carbon to chlorophyll a (C:Chl), and particulate N to particulate P (N:P) are illustrated in Figure 4C. In the upper mixed layer, NH_4 values were $0.5 \mu\text{M}$, chlorophyll a was $3 \mu\text{g l}^{-1}$, and particulate carbon was $50 \mu\text{M}$. An NH_4 maximum occurred at the depth of the temperature maximum. Minima in chlorophyll a and particulate carbon occurred where NH_4 was maximal. Below this zone, NH_4 values decreased to $1.5 \mu\text{M}$ before increasing to form the nutricline, and chlorophyll a and particulate carbon concentrations increased. The chlorophyll maximum occurred at 16 m depth. C:N and C:Chl ratios both had maxima at z_{TM} and decreased below 12 m depth (Fig. 4C). In contrast, N:P had a minimum at z_{TM} and increased below that depth.

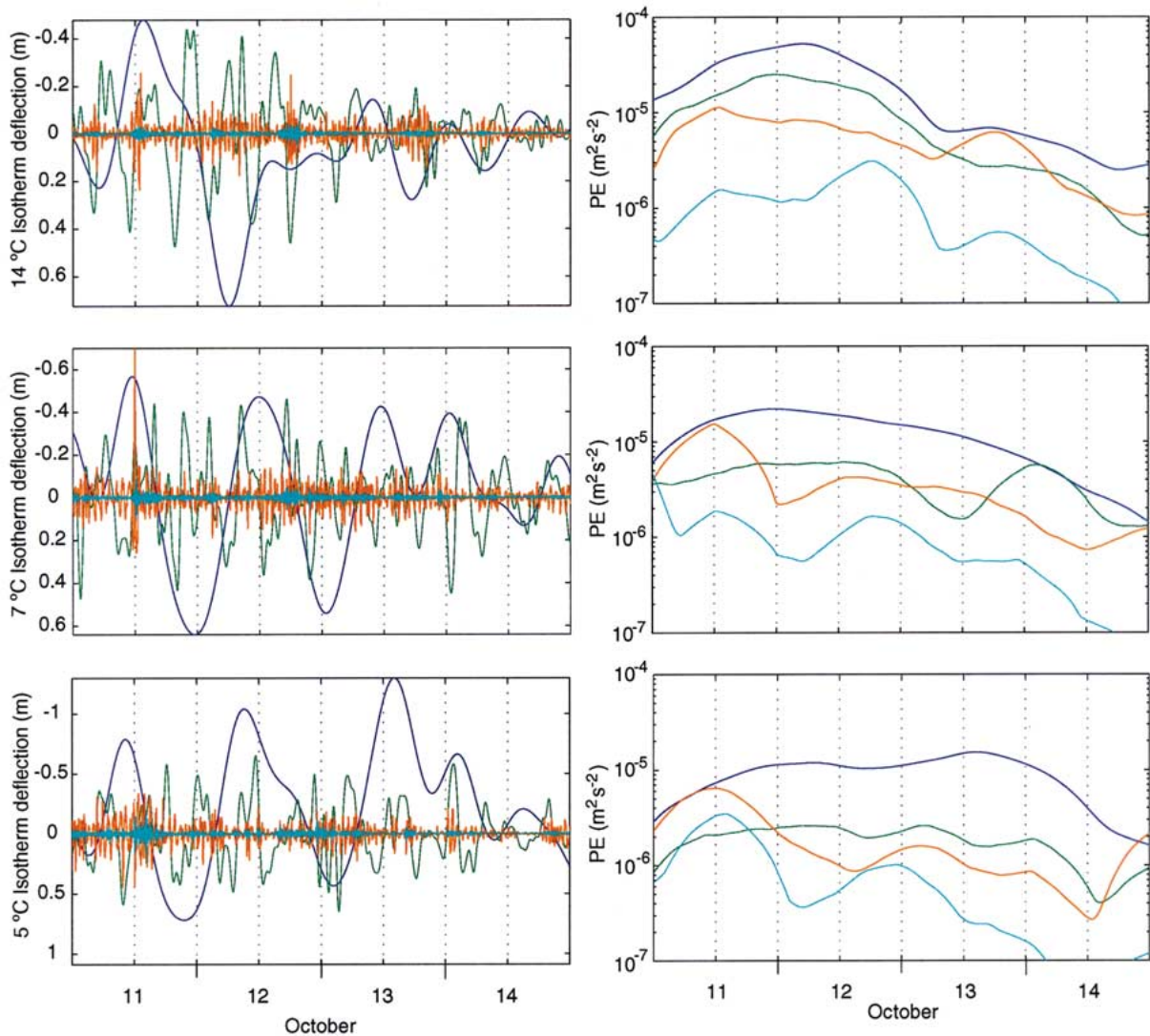


Figure 6. (A,C,E) 14 °C, 7 °C and 5 °C isotherms filtered to show contributions from different frequencies: 0.07–2.4 cpd (blue), 2.4–19.2 cpd (green), 19.2–192 cpd (red), and 192–600 cpd (turquoise). First frequency range includes basin scale waves; second contains harmonics of these waves, the first vertical first horizontal, and includes waves at critical frequencies for breaking; third range also is within range of critical frequencies; and fourth range is primarily above critical frequencies. (B, D, F). Potential energy per unit mass for the three isotherms in these four frequency bands showing decay over time. Window sizes are 24, 12, 12 and 12 h. Potential energy for the frequency band 19.2–192 cpd has been multiplied by 10; that in the band 192–600 cpd has been multiplied by 100.

Time series plots show that the ammonium maximum was broader and that concentrations were lower within it inshore than offshore (Fig. 8A,B). In particular, the maximum inshore spanned 4 m on the afternoon of 11 October. At both stations, concentrations were $0.3 \mu\text{m}$ or less in surface waters. Towards the end of the study, patches of water with higher NH_4 concentration appeared at the inshore station.

The chlorophyll minimum coincided with the NH_4 maximum at both inshore and offshore stations (Fig.

9). Inshore, it tended to be located at the upper boundary of the NH_4 maximum; offshore it tracked it more closely. Over the 4 days of measurements, the chlorophyll *a* values above 8 m depth inshore increased from $2 \mu\text{g l}^{-1}$ to $4 \mu\text{g l}^{-1}$ in the upper 8 m; offshore they increased from $3 \mu\text{g l}^{-1}$ to $4.5 \mu\text{g l}^{-1}$.

Similar patterns were observed at station 8, near the far north-eastern shore. A maximum in NH_4 also occurred at 10–11 m depth with lower concentrations below. NH_4 values in the upper mixed layer increased

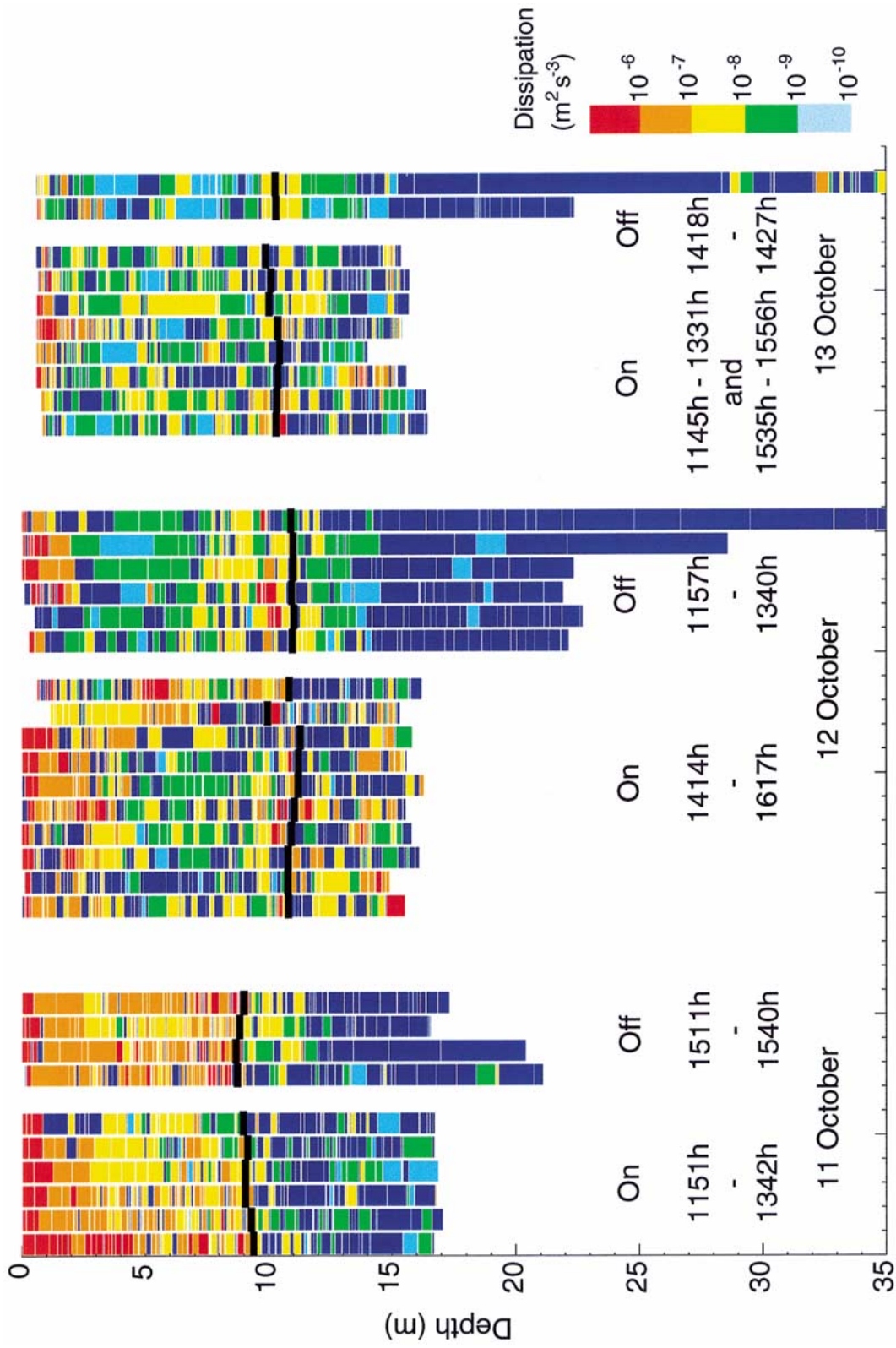


Figure 7. Rates of dissipation of turbulent kinetic energy at inshore and offshore stations on 11, 12 and 13 October 1995. Dissipations were highest in the upper 10 m on 11 October due to wind. On 12 October, the pycnocline has been energized at the inshore station, but only at the top of the pycnocline offshore. On 13 October, high turbulence is still present at the top of the pycnocline and at its base inshore; turbulence is less offshore in the pycnocline. Only segments with values of ϵ greater than $10^{-7} \text{ m}^2 \text{ s}^{-3}$ are sufficiently energized to support turbulent transport. Black line indicates z_{TM} . Last two profiles on 12 October were downcasts as were all on 13 October. Only two of the offshore casts extended to the bottom of the lake. Navy – not turbulent.

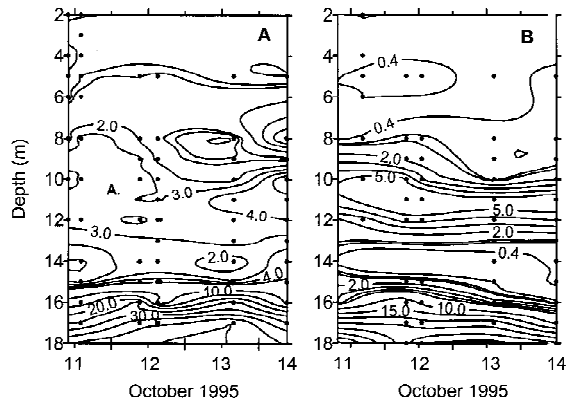


Figure 8. (A). NH_4 time series from 11 to 14 October at the inshore station showing the elevated concentrations near 10 m depth, an NH_4 minimum at 14 m depth, and the nutricline below 15 m depth. Upwelling is indicated by letter A. (B). As in A but at the offshore site. Contour intervals are $0.4 \mu\text{m}$, $0.8 \mu\text{m}$, $1 \mu\text{m}$ from 1 to $5 \mu\text{m}$, and $5 \mu\text{m}$ from 5 to $45 \mu\text{m}$. Inshore, the upwelling of NH_4 after the onset of high winds and the much greater dispersion of NH_4 both above and below the maximum at 10 m is apparent.

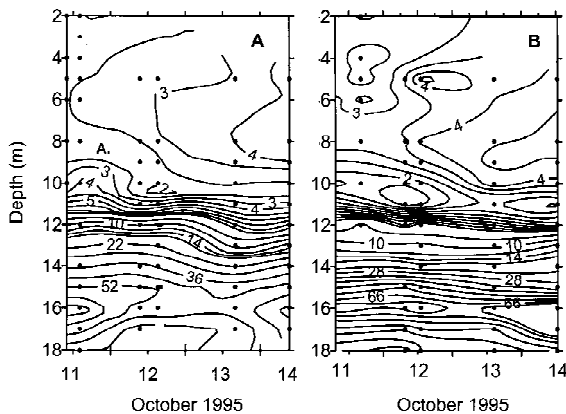


Figure 9. (A). As in Figure 8A but chlorophyll *a* concentrations inshore. The chlorophyll minimum co-occurs with the NH_4 maximum; chlorophyll *a* concentrations in the upper mixed layer increased after the strong wind forcing of 11–12 October. The upwelling on 11 October is illustrated (letter A) as are the increases in chlorophyll *a* in the mixed layer over the 4 days. (B). As in Figure 8B but chlorophyll *a* concentrations offshore. Contour intervals are $0.5 \mu\text{g l}^{-1}$ from 0 to $6 \mu\text{g l}^{-1}$, $2 \mu\text{g l}^{-1}$ from 6 to $16 \mu\text{g l}^{-1}$, $6 \mu\text{g l}^{-1}$ from 16 to $28 \mu\text{g l}^{-1}$, $8 \mu\text{g l}^{-1}$ from 28 to $60 \mu\text{g l}^{-1}$, and $4 \mu\text{g l}^{-1}$ from 60 to $70 \mu\text{g l}^{-1}$.

from $0.1 \mu\text{m}$ to $1 \mu\text{m}$ from 0830 h 11 October to 0820 h 12 October. Similarly, chlorophyll *a* increased from 2.8 to $5 \mu\text{g l}^{-1}$.

C:N molar ratios at the inshore station were always close to Redfield and not indicative of nutrient limitation, but did show a slight decrease over time (Fig. 10A). C:N molar ratios in the upper mixed layer offshore exceeded 9 at some depths on the first day of

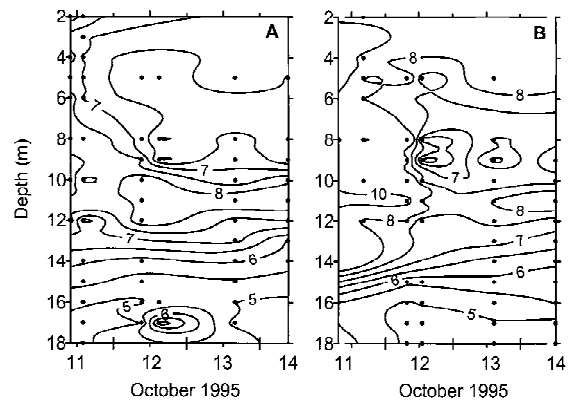


Figure 10. (A). As in Figure 8A but C:N molar ratios. (B). As in Figure 8B but C:N. Ratio is elevated at z_{TM} ; decrease in the upper mixed layer occurs over the four days. Greater decrease below 5 m and above z_{TM} indicates the upper mixed layer was not fully mixing. Contours are at 0.5 intervals from 4.5 to 8 with a step change to 10 offshore in panel B.

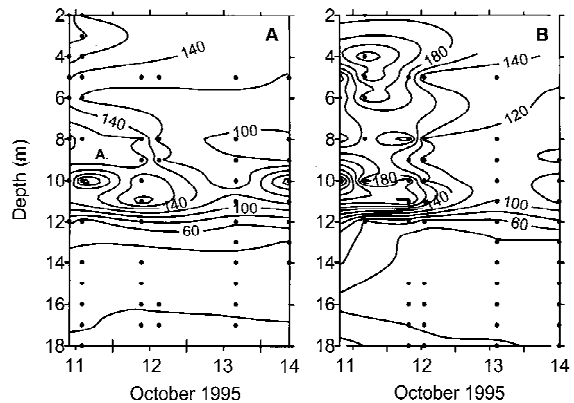


Figure 11. (A). As in Figure 8A but C:Chl weight ratios. Upwelling is indicated by letter A. (B). As in Figure 8B but C:Chl. Ratio is elevated at z_{TM} ; decrease in the upper mixed layer occurs over the 4 days. Greater decrease below 5 m and above z_{TM} indicates the upper mixed layer was not fully mixing. Contours are 20 weight:weight intervals.

sampling, values indicative of nutrient limitation. The ratio decreased to values near 7 over the four days (Fig. 10B). At both stations, highest values were observed at the temperature maximum; the ratio decreased below this depth. The decreases in the upper mixed layer occurred below 5 m depth.

C:Chl weight ratios were higher than 130 and suggestive of nutrient limited phytoplankton in the mixed layer inshore and offshore on the first day of sampling. The ratio decreased over time (Fig. 11A, B). At both stations, the decrease was largely below 5 m and above z_{TM} . The largest ratios occurred in the temperature maximum at both stations and also decreased over

Table 1. Abundance of adult *A. monica* on 14 October 1995

| Depth (m) | Adults m ⁻³ | Standard error |
|-----------|------------------------|----------------|
| 0-8 | 507 | 38 |
| 9 | 797 | 72 |
| 10 | 1033 | 146 |
| 11 | 797 | 68 |

time. The ratio was lower below z_{TM} and values were typical for nutrient replete, light limited cells.

Zooplankton

A. monica were sampled on 14 October at the offshore station using a vertical net haul for the upper 8 m and a Schindler trap at 9, 10 and 11 m (Table 1). The number of adults m⁻³ from 9 to 11 m was 70% higher than in the upper mixed layer.

Calculated fluxes of ammonia at the depth of the ammonia maximum

For vertical flux to occur, $\epsilon > 15\nu N^2$ (Ivey & Imberger, 1991). We determined whether the threshold was exceeded one meter above and one meter below the temperature maximum. Inshore, the percentage of segments in which dissipation rates exceeded the threshold on 11, 12 and 13 October were 39%, 72% and 45%, respectively. Offshore, the percentages were 76%, 12% and 20%. These calculations indicate that vertical transport at the top of the pycnocline would have been greatest offshore on the first day and lower thereafter; vertical transport would have been greater onshore on the second and third days. Had microstructure profiling at the inshore site occurred on 11 October after several hours of wind forcing, percentages may have been more similar to those at the offshore site.

We developed two approaches to compute lakewide estimates of the upward flux of ammonia. For the first approach, we assumed fluxes occurred on all days and weighted fluxes by multiplying by the percentage of segments in which the turbulence exceeded the threshold for mixing (Method A). We weighted the inshore and offshore fluxes by 20% and 80% based on the calculations in MacIntyre et al. (1999). For the second approach, we assumed that turbulence was only sufficiently energetic for turbulent transport at the offshore site on 11 October. This assumption was

based on the persistence of a high NH_4 gradient at the offshore site and because ϵ only exceeded the critical value for turbulent transport a significant fraction of the time on 11 October. Similarly, we assume that turbulence was sufficiently energetic for turbulent transport on 11 and 12 October at the inshore site. This assumption is based on the reduction in the nutrient gradient at the inshore station from 11 to 12 October, but its increase on the third day, and the higher percentages of ϵ greater than the threshold for turbulent flux on 12 October than 13 October. Consequently, we computed fluxes for 11 October using results from both stations, for 12 October using only the inshore station. (Method B). The areal weighting was as for Method A. The average flux over three days was 1.6 mmol m⁻² d⁻¹ using Method A and 1.1 mmol m⁻² d⁻¹ using Method B (Table 2).

Discussion

Major progress in understanding physical controls on lacustrine ecosystem dynamics will occur when we can relate the onset, spatial variability and intensity of turbulence to wind forcing and the resulting internal wave field. Power spectra from our data clearly show the higher energy content in the wave field after persistent, high winds on 11 October and the subsequent decline in energy (Fig. 5). Rates of dissipation of turbulent kinetic energy were higher at the top of the pycnocline on the first 2 days of the study and were highest at the top and base of the pycnocline at the inshore site on the second day. Both the power spectra, the filtered data, and the potential energies indicate the energy in the wave field was elevated over a broad range of frequencies after wind forcing (Figs 5 and 6).

Expansion of the ideas developed in Monismith (1985) may lead to new insights. Monismith showed that the magnitude of shear depends on the phase between waves on different interfaces. The largest shears occur when isopycnal surfaces become level in the transition between the pycnocline's up and downwelling (Monismith, 1985). Such shears may be sufficient to induce turbulence. Monismith's analysis was restricted to a three-layer model of a lake's stratification and to the first two vertical mode internal waves. However, stratification within lakes is much more complex. Not only can higher order vertical wave modes be supported by these stratifications (LaZerte, 1980), but also harmonics of the horizontal modes. In consequence, the movement of adjacent

Table 2. Flux of ammonia away from the NH_4 maximum in Mono Lake. $F = K_z \partial[\text{NH}_4]/\partial z$ where K_z is the arithmetic average in 1 m bin. Calculations were done within the NH_4 maximum at depths where the concentration gradient was maximal. I indicates inshore data used in the calculation; O, offshore. Lakewide fluxes are computed when turbulence is sufficiently energetic to cause vertical fluxes.

| | Depth (m) | ΔNH_4 μMm^{-1} | K_z $\text{m}^2 \text{s}^{-1}$ | Flux mmoles $\text{m}^{-2} \text{d}^{-1}$ | Lakewide Flux (A) mmoles $\text{m}^{-2} \text{d}^{-1}$ | Lakewide Flux (B) mmoles $\text{m}^{-2} \text{d}^{-1}$ |
|---------------------------|--------------|--|-------------------------------------|---|---|---|
| Inshore | | | | | | |
| 11 Oct 1410 h | 6–8 | 1.1 | 1.3×10^{-5} | 1.2 | 2.2 | 3, IO |
| 12 Oct 0925 h | 9–10 | 0.7 | 1.3×10^{-5} | 1.1 | 1.9 | 0.2, I |
| 13 Oct 1600 h | 10–11 | 3.3 | 1.6×10^{-6} | 0.45 | 0.6 | 0.0 |
| Offshore | | | | | | |
| 11 Oct 1620 h | 8–10 | 2.5 | 1.6×10^{-5} | 3.4 | | |
| 12 Oct 1310 h | 10–11 | 3.8 | 5.7×10^{-5} | 18.7 | | |
| 13 Oct 1445 h | 10–11 | 5 | 8.7×10^{-6} | 3.7 | | |
| Three-day average flux | | | | | 1.6 | 1.1 |

isopycnals may frequently be out of phase causing intermittent increases in shear. Consequently, turbulence may be intermittently generated by the mechanism of shear instability.

A full exploration of these ideas is beyond the scope of this paper, but phase differences between adjacent isopycnals were present. For example, at ca. 0200 h 13 October, the 6 °C isotherm downwells ca. 0.75 m, while the 7 °C isotherm remains nearly level (Fig. 3B). Such differences in movement may lead to shear. Phase differences between waves in different frequency bands are illustrated in Figure 6A,C, E. For instance, while the lowest frequency waves comprising the 7 and 5 °C isopycnals are nearly in phase at 0000 h 13 October, the waves in the 2nd lowest band go through essentially one up and downwelling cycle from 0000 h to 0200 h on the 7 °C isotherm while they go through three such cycles on the 5 °C isopycnal. These differences in frequency lead to the phase differences between isotherms, as observed between the 7 °C and 6 °C isotherms in Figure 3B, and may contribute to steppiness in the pycnocline as observed inshore and to the development of shear and subsequent turbulence.

Waves of different frequencies could also be caused by the interaction of basin-scale waves with topography, and their interaction with the ambient density field could lead to enhanced turbulence (Thorpe, 1998). For example, steppiness can be generated in the pycnocline due to the interaction of the ambi-

ent density field with lee waves which are generated by the interaction of larger scale waves with topographic features (Thorpe, 1998). The step-like features in the pycnocline inshore on 12 and 13 October, with enhanced dissipation rates associated with the steps, provide evidence that such interactions may be occurring in Mono Lake. Step-like features may also be due to intrusions as would result from wave breaking inshore and flow of the well mixed water along isopycnals offshore.

Dissipation rates were also high at the top of the pycnocline both inshore and offshore. We do not have time series temperature data there to help define the mechanisms likely to have generated the turbulence. The turbulence may have been due to shear instability with shear generated due to the initial upwelling of basin scale waves. The magnitude of the Turner angle indicates that double diffusive convection may also have contributed to turbulence at the top of the pycnocline (MacIntyre et al., 1999).

In summary, we observed enhanced turbulence at the top of the pycnocline both inshore and off when internal wave amplitudes increased due to strong wind forcing. Turbulence was enhanced throughout the pycnocline inshore on the second and third days after the initial wind forcing. We now combine these data with our chemical and biological observations to address the question of when and where vertical fluxes of NH_4 occurred and the consequences for phytoplankton in Mono Lake.

The persistent ammonium maximum

Ammonium profiles consistently show that the highest concentration of ammonium occurred within a meter of the temperature maximum and that this feature persisted over a 4-day period despite enhanced turbulence at those depths. Changes in concentration over time depend on sources, sinks and vertical fluxes, and we do not have sufficient data to construct a full budget. For instance, quantifying uptake of N by phytoplankton would have required measurements at the time of the experiment. However, we can evaluate sources and vertical fluxes. If the fluxes due to turbulent mixing were large relative to the sources, we would not expect the NH_4 maximum to persist. We can determine whether sufficient ammonium was mixed vertically to affect nutrient limitation by phytoplankton.

Sources

Sources of NH_4 include excretion by *A. monica*, enhanced diffusive fluxes at the sediment water interface, advection or excretion by microzooplankton. Data on microzooplankton are not available. Excretion rates of NH_4 by adult *A. monica* are $0.6 \mu\text{mole d}^{-1}$ (Jellison et al., 1993). With an average abundance of *A. monica* of $876 \text{ adults m}^{-3}$ at the depths of the temperature maximum, the flux into a 1 m^3 parcel of water would be $0.5 \text{ mmoles m}^{-3} \text{ d}^{-1}$. Juvenile *A. monica* were not present in sufficient numbers to contribute to the ammonium pool. Previous lake wide sampling has indicated that the maximum numbers of brine shrimp can range from 500 to 3000 adults m^{-3} (Lenz, 1980). Were such a wide range present during our sampling, maximum fluxes of NH_4 could be up to $1.8 \text{ mmoles m}^{-3} \text{ d}^{-1}$.

Jellison et al. (1993b) estimated diffusive fluxes from the sediments at depths below the nutricline to be $6 \text{ mmoles m}^{-2} \text{ d}^{-1}$. Data are not available to calculate fluxes from sediments above the nutricline. Were they comparable, the flux into a 1 m layer spanning the whole lake would be $2 \mu\text{moles m}^{-3} \text{ d}^{-1}$, a flux three orders of magnitude too low to account for the higher NH_4 at those depths. Shear stresses at the sediment-water interface may enhance the fluxes, but at present, theoretical models indicate at most a three-fold increase due to turbulence at the benthic boundary layer (Dade, 1993). Advection of water with higher NH_4 content could contribute to persistence of the feature, but our data do not show large spatial differences in NH_4 concentrations.

Based on these comparisons, we infer that the high concentrations of NH_4 at the top of the pycnocline

resulted from excretion by adult *A. monica*. The elevated concentrations could only have persisted if the vertical fluxes of NH_4 due to turbulence were less than the NH_4 excretion rates and if uptake rates by phytoplankton or bacteria were low.

Vertical fluxes

Several lines of evidence suggest that vertical fluxes of NH_4 occurred and that turbulent transport may have been greater at inshore sites than offshore sites. The time series measurements of temperature, NH_4 , chlorophyll *a* and C:Chl indicate upwelling occurred inshore on 11 October but not offshore. This upwelling, coupled with the enhanced turbulence at the depths of upwelling, may have contributed to the greater spread of NH_4 in the NH_4 maximum and of chlorophyll *a* in the chlorophyll *a* minimum (Figs 8 and 9). Increased spread of a solute and slightly lower maximum concentrations are to be expected when mixing has occurred. Chlorophyll *a* is more dispersed inshore below 12 m depth.

For vertical mixing to occur and to cause transport across isopycnals, dissipation rates must be high enough to exceed the damping induced by viscous and buoyancy forcing. Dissipation rates were sufficiently high at the top of the pycnocline 76% of the time offshore but less than 20% of the time on the next 2 days. Inshore, dissipation rates were sufficiently high 72% of the time on the second day and 45% of the time on the third day. Temperature profiles with millimeter scale resolution indicated that temperature inversions with scales of centimeters were present when ϵ was large enough to cause transport. Inversions were on smaller scales or not present when it was less than $15 \nu N^2$ (S. MacIntyre, unpublished data). Consequently, when ϵ exceeded the threshold, turbulent overturns l occurred allowing vertical transport.

Calculated daily vertical fluxes of NH_4 at the offshore site are higher than likely excretion rates (Table 2). We assume the flux is into a 1 m^3 volume for comparison with the *A. monica* excretion rates. The calculated fluxes were particularly high on days when ϵ was frequently below the threshold for vertical transport and when the NH_4 gradient remained high. These results suggest vertical fluxes, calculated as $F = K_z \partial[\text{NH}_4]/\partial z$, were much less than calculated. The discrepancy indicates that calculating K_z as $\Gamma \epsilon N^{-2}$ (Osborn, 1980) is not always valid. It-sweire et al. (1993) found that the assumptions of Osborn's (1980) model were not met when stratification and viscosity were high relative to the forces

that would generate turbulence. In contrast, calculated daily fluxes at the inshore site could be supported by excretion by *A. monica*. Inshore a greater percentage of the dissipation rates exceeded the threshold for turbulent transport; consequently Osborn's model was applicable for calculating K_z .

Vertical fluxes and phytoplankton growth

In comparison to the quantity of ammonia excreted by *A. monica*, the calculated lake-wide fluxes of NH_4 are reasonable although at the upper end of the range possible (Table 2). As these calculated fluxes take into account the percentage of the time that turbulence is sufficiently high to overcome damping forces, we use them to estimate the possible growth of phytoplankton. Using a C:N molar ratio of 7, the lower of the three day averages, $1.1 \text{ mmol m}^{-2} \text{ d}^{-1}$, the fluxes would have supported primary productivities of $0.1 \text{ g C m}^{-2} \text{ d}^{-1}$. Daily rates of primary production are between 0.5 and $2 \text{ g C m}^{-2} \text{ d}^{-1}$ during the summer in Mono Lake (Jellison & Melack, 1993a). The fluxes would have provided sufficient NH_4 to support 5–20% of the daily requirements for growth.

Growth will only occur at depths to which the NH_4 is mixed. Persistence of thermal stratification in the upper mixed layer and ϵ only consistently exceeding the threshold for vertical mixing in the upper 5 m indicates the upper mixed layer did not fully mix (MacIntyre et al., 1999, MacIntyre, unpublished data). Consequently, the vertical fluxes of NH_4 will be into a limited volume and growth or reduction of nutrient limitation will not occur throughout the entire upper mixed layer. To further determine whether vertical fluxes of NH_4 occurred, we determine whether there was evidence for alleviation of nutrient limitation or for growth.

Vertical fluxes of NH_4 and changes in nutrient limitation and abundance of chlorophyll

C:N ratios and C:Chl ratios decreased at depths above the temperature maximum at all sites over the course of the study (Figs 10 and 11). The decrease in the C:N ratio in the upper mixed layer at the offshore station provided the strongest evidence for a reduction in nutrient limitation. C:N molar ratios above 8.3 indicate waters that are moderately N deficient (Guildford & Hecky, 2000), and offshore waters initially had C:N molar ratios in excess of 9. In contrast, the ratios in the upper mixed layer inshore do not indicate nutrient

limitation during this experiment. Decreases occurred below 5 m depth.

Jellison & Melack (2001) illustrate the seasonal variation of C:Chl weight ratios in Mono Lake. Ratios above 200 occur in summer when phytoplankton are most nutrient stressed. Ratios decline in the autumn due to the onset of vertical mixing and have the lowest values in winter. Frenette et al. (1996) attribute a decrease in C:Chl from a range of 100–150 to a range of 50–100 to increased intracellular chlorophyll after a wind event caused resuspension of sediments and nutrient rich pore waters. They reasoned that resuspension of non-algal material would increase the C:Chl ratio, and that the reduction was therefore indicative of increased chlorophyll in phytoplankton cells. An alternate explanation for a decrease in the C:Chl ratio is vertical mixing of dark adapted phytoplankton cells into the upper mixed layer. For instance, for cells grown in cultures at high light the ratio was around 100, at low light, 20 (Cullen & Lewis, 1988).

Depending on the time scale for photoadaptation, a decrease in the ratio in surface waters could indicate upward mixing of dark-adapted cells with higher intracellular chlorophyll. Because a minimum in chlorophyll *a* occurred at the depths where ϵ was highest, we do not believe the decreased ratio we observed was due to transport of dark-adapted cells from deeper in the pycnocline into the upper mixed layer. The decrease reflected either growth of phytoplankton or growth of chloroplasts within individual cells. Again, the decrease in the ratio occurred below 5 m depth and above z_{TM} .

Over the 4 days, chlorophyll *a* abundance doubled in the upper mixed layer at the inshore station and increased by 30–50% offshore. Advection could have led to the observed changes in biomass if the gyre (Melack & Gastil, this volume; Melack, in press) in the northeastern section of the lake on 10 October shifted its position due to wind forcing or was dispersed. On 10 October, chlorophyll concentrations in the gyre ranged from 2.8 to $4.3 \mu\text{g l}^{-1}$. Station 8, just on the south-eastern edge of the feature, had a chlorophyll *a* concentration of $2.9 \mu\text{g l}^{-1}$, and concentrations at stations 5 and 6 were $2.2 \mu\text{g l}^{-1}$ and $1.9 \mu\text{g l}^{-1}$, respectively. Movement of the gyre could account for the increased biomass observed at our study sites. Inside the gyre the C:N ratio was ~ 12 and C:Chl ratios exceeded 170. These values indicated the phytoplankton in the gyre were nutrient limited. Consequently, the decreases in these ratios at our study sites indicate

that alleviation of nutrient limitation was not due to advection but to vertical mixing of NH_4 .

In summary, changes in C:N and C:Chl ratios indicate that vertical fluxes of ammonium occurred. Vertical fluxes of NH_4 were induced by increased potential energy in the internal wave field due to wind forcing. After the initial wind forcing, fluxes were more likely to occur inshore. While these fluxes were sufficient to cause slight increases in growth, they did lead to suppression of nutrient limitation and an increase in chlorophyll within phytoplankton cells. Consequently, an initial strong wind forcing event reduced nutrient limitation which could permit subsequent growth if fluxes of nutrients continued from vertical mixing or *A. monica* excretion. The ratios decreased more at the base of the upper mixed layer indicating that it never fully mixed. Enhanced growth would be most likely to occur at those depths.

Within the temperature maximum, NH_4 values stayed fairly constant, particulate C as well as chlorophyll *a* was always lower than in the water immediately above and below, and the C:Chl weight ratio decreased. On 14 October, *A. monica* abundance was highest where NH_4 concentrations were highest. Consequently their grazing and excretion may explain the changes in the concentrations of NH_4 , chlorophyll *a* and particulate carbon within the temperature maximum. At the beginning of our sampling period, the water was nearly anoxic at 12 m depth, and algal biomass increased at 12 m. Hence, the zooplankton may have initially been abundant at a depth above 12 m where oxygen concentrations were sufficient and abundances of phytoplankton were higher than in overlying waters. The turbulence in the metalimnion would have continued to supply the *A. monica* with phytoplankton. The decrease in the C:Chl ratio at that depth may reflect the upward mixing of dark adapted phytoplankton cells.

Persistent layering

Thin layers of phytoplankton, zooplankton and nutrients that extend for kilometers have recently been observed in coastal waters and fjords (Cowles & Desiderio, 1993; Hanson & Donaghay, 1998; Alldredge et al., in press.). Bacteria also accumulate in the layers, and layers of particulate organic matter are elevated at the same depths as these layers or slightly below. Typically the layers are associated with density discontinuities (MacIntyre et al., 1995). Turbulent intensities are too low and turbulent eddies are too small

to disrupt them (Alldredge et al., in press.). In fact, turbulence is often higher on their boundaries than within them, indicating that the layers are flowing between other water masses as intrusions. Our finding a layer with elevated NH_4 and abundant zooplankton in Mono Lake is another example of persistent layering over space and time. It persisted because the turbulence was intermittent, and did not remain at intensities sufficient to cause vertical transport.

Summary

Intermittent transport and mixing events are critical for resupply of nutrients to the euphotic zone in stratified water bodies. Mechanisms of supply include upwelling (Coulter & Spigel, 1991; Ostrovsky et al., 1996), boundary mixing (Goudsmit et al., 1997; MacIntyre et al., 1999), shear and static instability of internal waves (Thorpe, 1978, 1994), entrainment caused by wind mixing or heat loss by convection (MacIntyre & Melack, 1995), differential heating and cooling (James & Barko, 1991; Nepf & Oldham, 1997), and sediment resuspension with subsequent advection (Robarts et al., 1998). Our study indicates that the energy supplied by the wind energizes the internal wave field, that energy decays rapidly, and that the resulting turbulence occurs over a limited period of time. Initially the turbulence occurred at the top of the pycnocline inshore and offshore, but later the turbulence was greater inshore. Vertical transport of nutrients occurred when dissipation rates were sufficient to overcome viscous and buoyancy forces. At those times, turbulent mixing caused sufficient nutrient flux to alleviate nutrient limitation and to support modest growth. This improved physiological state could lead to increased growth were fluxes to continue. While strong wind events occur infrequently in the autumn in Mono Lake, frontal systems with high winds are frequent in the spring and a strong diurnal wind pattern sets up in the summer. In these other seasons, wind forcing may lead to injections of limiting nutrients and enhanced growth. Similar scenarios are likely in other lakes. In addition, spatial-temporal variations in vertical mixing and its limited vertical extent abets structuring of biological communities despite strong wind forcing. Rates of biological and chemical processes may differ inshore and off.

Acknowledgements

We thank Darla Heil, Mike Emory, Pete Kirchner and Kevin Flynn for their help with field work and chemical processing. Manuela Lorenzi-Kayser, Kevin Flynn and Lorenz Moosmann helped with data processing, programming, and graphics. Mary Gastil provided essential information regarding the gyre. We thank William Shaw for assistance with signal processing techniques, G.W. Kling and L. Moosmann for helpful comments, and E.E. McPhee, W. Shaw and J.M. Melack for critically reading the manuscript. The Centre for Water Research, University of Western Australia, provided the software for microstructure analysis. We thank Michael Head for his technical support of the microstructure profilers.

Financial support was provided by NSF Grants DEB93-17986, DEB97-26932, and OCE99-06924 to S.M. and DEB95-08733 to R.J. and J.M. Melack. Logistic support was provided by the Sierra Nevada Aquatic Research Laboratory, University of California Natural Reserve System.

References

- Allredge, A. L., T. J. Cowles, S. MacIntyre, J. E. B. Rines, P. L. Donaghay, C. F. Greenlaw, D. V. Holliday, M. M. Deksheniks, J. M. Sullivan & J. R. V. Zaneveld, in press. Occurrence and mechanisms of formation of a dramatic thin layer of marine snow in a shallow Pacific fjord. *Mar. Ecol. Prog. Ser.*
- Coulter, G. W. & R. H. Spiegel, 1991. Hydrodynamics. Chapter 3 In Coulter, G. W. (ed.), *Lake Tanganyika and its Life*. Oxford Univ. Press: 49–75.
- Cowles, T. J. & R. A. Desiderio, 1993. Resolution of biological microstructure through *in situ* fluorescence emission spectra. *Oceanography* 6: 105–111.
- Cullen, J. J. & M. R. Lewis, 1988. The kinetics of algal photoadaptation in the context of vertical mixing. *J. Plankton Res.* 10: 1039–1063.
- Dade, W. B., 1993. Near-bed turbulence and hydrodynamic control of diffusional mass transfer at the sea floor. *Limnol. Oceanogr.* 38: 52–69.
- DeSilva, I. P. D., J. Imberger & G. N. Ivey, 1997. Localized mixing due to a breaking internal wave ray at a sloping bed. *J. Fluid Mech.* 350: 1–27.
- Dillon, T. M. & D. R. Caldwell, 1980. The Batchelor spectrum and dissipation in the upper ocean. *J. Geophys. Res.* 85: 1910–1916.
- Etamad-Shahidi, A. & J. Imberger, 2001. Anatomy of turbulence in thermally stratified lakes. *Limnol. Oceanogr.* 46: 1158–1170.
- Frenette, J. J., W. F. Vincent, L. Legendre & T. Nagata, 1996. Size-dependent phytoplankton responses to atmospheric forcing in Lake Biwa. *J. Plankton Res.* 18: 371–391.
- Gloor, M., A. Wuest & M. Munnich, 1994. Benthic boundary mixing and resuspension induced by internal seiches. *Hydrobiologia* 284: 59–68.
- Golterman, H. L., 1969. *Methods for Chemical Analysis of Fresh Waters*. International Biological Program Handbook. No. 8. Blackwell Scientific Publications, Oxford: 166 pp.
- Goudsmit, G.-H., F. Peeters, M. Gloor & A. Wuest, 1997. Boundary versus internal diapycnal mixing in stratified natural waters. *J. Geophys. Res.* 102: 27903–27914.
- Guildford, S. J. & R. E. Hecky, 2000. Total nitrogen, total phosphorus, and nutrient limitation in lakes and oceans: is there a common relationship? *Limnol. Oceanogr.* 45: 1213–1223.
- Hanson, A. K. & P. L. Donaghay, 1998. Micro- to fine-scale chemical gradients and layers in stratified coastal waters. *Oceanography* 11: 10–17.
- Imberger, J., 1985. The diurnal mixed layer. *Limnol. Oceanogr.* 30: 737–770.
- Imberger, J. & G. Ivey, 1991. On the nature of turbulence in a stratified fluid. Part 2: application to lakes. *J. Phys. Oceanogr.* 21: 659–680.
- Imberger, J. & J. Patterson, 1990. Physical limnology. *Adv. Appl. Mech.* 27: 303–475.
- Itsweire, E. C., J. R. Koseff, D. A. Briggs & J. H. Ferziger, 1993. Turbulence in stratified shear flows – implications for interpreting shear-induced mixing in the ocean. *J. Phys. Oceanogr.* 23: 1508–1522.
- Ivey, G. & J. Imberger, 1991. On the nature of turbulence in a stratified fluid. Part 1: the efficiency of mixing. *J. Phys. Oceanogr.* 21: 650–658.
- James, W. F. & J. W. Barko, 1991. Littoral-pelagic phosphorus dynamics during night-time convective circulation. *Limnol. Oceanogr.* 31: 900–906.
- Jassby, A. & T. M. Powell, 1975. Vertical patterns of eddy diffusion during stratification in Castle Lake, California. *Limnol. Oceanogr.* 38: 1008–1019.
- Jellison, R. S. & J. M. Melack, 1988. Photosynthetic activity of phytoplankton and its relation to environmental factors in hypersaline Mono Lake, California. *Hydrobiologia* 158: 69–88.
- Jellison, R. S. & J. M. Melack, 1993a. Algal photosynthetic activity and its response to meromixis in hypersaline Mono Lake, California. *Limnol. Oceanogr.* 38: 818–837.
- Jellison, R. S. & J. M. Melack, 1993b. Meromixis in hypersaline Mono Lake, California. 1: Vertical mixing and density stratification during the onset, persistence and breakdown of meromixis. *Limnol. Oceanogr.* 38: 1008–1019.
- Jellison, R. S. & J. M. Melack, 2001. Nitrogen limitation and particulate elemental ratios of seston in hypersaline Mono Lake, California, U.S.A. *Hydrobiologia* 466 (Dev. Hydrobiol. 162): 1–12.
- Jellison, R. S., L. Miller, J. M. Melack & G. L. Dana, 1993. Meromixis in hypersaline Mono Lake, California. 2: Nitrogen fluxes. *Limnol. Oceanogr.* 38: 1020–1039.
- Jellison, R., S. MacIntyre & F. J. Millero, 1999. Density and conductivity properties of Na-CO₃-Cl-SO₄ brine from Mono Lake, California. *Int. J. Salt Lake Res.* 8: 41–53.
- LaZerte, B., 1980. The dominating higher order vertical modes of the internal seiche in a small lake. *Limnol. Oceanogr.* 25: 846–854.
- Ledwell, J. R., E. T. Montgomery, K. L. Polzin, L. C. St. Laurent, R. W. Schmitt & J. M. Toole, 2000. Evidence for enhanced mixing over rough topography in the abyssal ocean. *Nature* 403: 179–182.
- Lenz, P., 1980. Ecology of an alkali-adapted variety of *Artemia* from Mono Lake, California, U.S.A. In Persoone, G., P. Sorgeloos, O. Roels & E. Jaspers (eds), *The Brine Shrimp Artemia*. Vol. 3. Ecology, Culturing. Use in Aquaculture. Universa Press, Wetteren, Belgium: 79–96.

- Lueck, R. G. & T. D. Mudge, 1997. Topographically induced mixing around a shallow seamount. *Science* 276: 1831–1833.
- MacIntyre, S., 1993. Vertical mixing in a shallow eutrophic lake: possible consequences for the light climate of phytoplankton. *Limnol. Oceanogr.* 38: 798–817.
- MacIntyre, S., 1998. Turbulent mixing and resource supply to phytoplankton. In Imberger, J. (ed.), *Physical Processes in Lakes and Oceans, Coastal and Estuarine Studies*, AGU: 539–567.
- MacIntyre, S., A. L. Alldredge & C. C. Gotschalk, 1995. Accumulation of marine snow at density discontinuities in the water column. *Limnol. Oceanogr.* 40: 449–468.
- MacIntyre, S. & J. M. Melack, 1995. Vertical and horizontal transport in lakes: linking littoral, benthic and pelagic habitats. *J. n. am. Benthol. Soc.* 14: 599–615.
- MacIntyre, S., K. M. Flynn, R. Jellison & J. R. Romero, 1999. Boundary mixing and nutrient flux in Mono Lake, CA. *Limnol. Oceanogr.* 44: 512–529.
- MacIntyre, S. & J. R. Romero, 2000. Predicting upwelling, boundary mixing, and nutrient fluxes in lakes. *Verh. int. Ver. Limnol.* 27: 246–250.
- Maxworthy, T., J. Imberger & A. Saggio, 1998. A laboratory demonstration of a mechanism for the production of secondary, internal gravity-waves in a stratified fluid. In Imberger, J. (ed.), *Physical Processes in Lakes and Oceans. Coastal and Estuarine Studies*, AGU: 261–270.
- Melack, J. M., (in press). Ecological dynamics in saline lakes. *Verh. int. Ver. Limnol.*
- Melack, J. M. & R. Jellison, 1998. Limnological conditions in Mono Lake: Contrasting monomixis and meromixis in the 1990s. *Hydrobiologia* 384: 21–39.
- Melack, J. M. & M. Gastil, 2001. Airborne remote sensing of chlorophyll distributions in Mono Lake, California. *Hydrobiologia* 466 (Dev. Hydrobiol. 162): 31–38.
- Monismith, S. G., 1985. Wind-forced motions in stratified lakes and their effect on mixed-layer shear. *Limnol. Oceanogr.* 30: 771–783.
- Moum, J. N., D. Hebert, C. A. Paulson & D. R. Caldwell, 1992. Turbulence and internal waves at the equator. Part I. Statistics from towed thermistors and a microstructure profiler. *J. Phys. Oceanogr.* 22: 1330–1345.
- Nepf, H. M. & C. E. Oldham, 1997. Exchange dynamics of a shallow contaminated wetland. *Aquat. Sci.* 59: 193–213.
- Oakey, N., 1985. Statistics of mixing parameters in the upper ocean during JASIN Phase 2. *J. Phys. Oceanogr.* 15: 1662–1675.
- Osborn, T. R., 1980. Estimates of the rate of vertical diffusion from dissipation measurements. *J. Phys. Oceanogr.* 10: 83–89.
- Ostrovsky, I., Y. Z. Yacobi, P. Walline & I. Kalikhman, 1996. Seiche-induced mixing – its impact on lake productivity. *Limnol. Oceanogr.* 41: 323–332.
- Patterson, J. C., 1991. Modelling the effects of motion on primary production in the mixed layer of lakes. *Aquat. Sci.* 53: 218–238.
- Polzin, K. L., J. M. Toole, J. R. Ledwell & R. W. Schmidt, 1997. Spatial variability in turbulent mixing in the abyssal ocean. *Science* 276: 93–96.
- Roberts, R. D., M. Waiser, O. Hadas, T. Zohary & S. MacIntyre, 1998. Contrasting relaxation of phosphorus limitation due to typhoon-induced mixing in two morphologically distinct basins of Lake Biwa, Japan. *Limnol. Oceanogr.* 43: 1023–1036.
- Romero, J. R. & J. M. Melack, 1996. Sensitivity of vertical mixing in a large saline lake to variations in runoff. *Limnol. Oceanogr.* 41: 955–965.
- Romero, J. R., R. Jellison & J. M. Melack, 1998. Stratification, mixing and ammonia flux in a hypersaline lake. *Archiv. Hydrobiol.* 142: 283–315.
- Saggio, A. & J. Imberger, 1998. Internal wave weather in a stratified lake. *Limnol. Oceanogr.* 1780–1795.
- Saggio, A. & J. Imberger, 2001. Mixing and turbulent fluxes in the metalimnion of a stratified lake. *Limnol. Oceanogr.* 46: 392–409.
- Strickland, J. S. H. & T. R. Parsons, 1972. A practical handbook of seawater analysis. *Bull. Fish. Res. Bd Can.* 167: 1–130.
- Svensson, U., 1978. Examination of the summer stratification. *Nordic Hydrology* 9(2).
- Tennekes, H. & J. L. Lumley, 1972. *A First Course in Turbulence*. MIT Press: 300 pp.
- Thorpe, S. A., 1978. On the shape and breaking of finite amplitude internal gravity waves in a shear flow. *J. Fluid Mech.* 85: 7–31.
- Thorpe, S. A., 1984. A laboratory study of stratified accelerating shear flow over a rough boundary. *J. Fluid Mech.* 138: 185–196.
- Thorpe, S. A., 1987. On the reflection of a train of finite-amplitude internal waves from a uniform slope. *J. Fluid Mech.* 178: 279–302.
- Thorpe, S. A., 1989. The distortion of short internal waves produced by a long wave, with applications to ocean boundary mixing. *J. Fluid Mech.* 208: 395–415.
- Thorpe, S. A., 1994. Statically unstable layers produced by overturning internal gravity waves. *J. Fluid Mech.* 260: 333–350.
- Thorpe, S. A., 1998. Some dynamical effects of the sloping sides of lakes. In Imberger, J. (ed.), *Physical Processes in Lakes and Oceans. Coastal and Estuarine Studies*, AGU: 441–460.
- Wuest, A., G. Piepke & D. C. Van Senden, 2000. Turbulent kinetic energy balance as a tool for estimating eddy diffusivity in wind-forced stratified waters. *Limnol. Oceanogr.* 45: 1388–1400.